School of Physics and Astronomy

Evolved Stellar Populations with James Webb Space Telescope

Conor Nally
May 24, 2022

Abstract

Evolved stellar populations are an excellent tracer for galactic metallicity and star formation history. During the thermally-pulsing phase of the Asymptotic Giant Branch (TP-AGB) they exhibit large mass loss rates which eventually consume the entire stellar envelope. Some of the material thrown off condenses into dust which obscures the light emitted by the star, making them difficult to observe. The launch of *JWST* is expected to make breakthroughs in revolved stellar studies, allowing us to probe further than the immediate neighbours of the Milky Way and deep into the Local Volume. Observing a wider range of galaxies that offer chemical conditions similar to earlier in the universe, offer us a greater understanding of the chemical enrichment cycles through history.

Signature: **ConorNally** Date: 24-5-2022

Supervisor: Dr. Olivia Jones, Prof. Annette Ferguson

Contents

1 Introduction

We will shortly be entering a golden age for evolved stellar population studies in Local Volume galaxies. The James Webb Space Telescope (JWST) is expected to lead to many breakthroughs in our understanding of this enigmatic phase of stellar evolution. Its primary mirror is nearly 8 times the diameter of NASAs' previous flagship infrared observatory *Spitzer*. Whereas *Spitzer* offered groundbreaking depth in its time, it was limited to galactic objects within a few Mpc, *JWST* will receive a similar stunning resolution of bright evolved stars out past 40 Mpc. This opens up a huge new area of exploration, offering galactic objects with a wide range of properties to study. We have already had previews of the huge increase in sensitivity during the current calibration stage (Figure 1).

Dust enshrouded evolved stars play a vital role in the chemical enrichment cycle of a galaxy. Dominated by a phase of strong dust driven mass loss, We can observe the matter they inject into the interstellar medium and their abundance traces intermediate star formation histories. By identifying resolvable galaxies within the Local Volume with a range of properties, we can use them as analogues for galaxies stretching back in history. Analysis of the evolved stars within them allows us to gain a strong insight into the chemical enrichment process and how their evolution be be affected during different epochs of the universe.

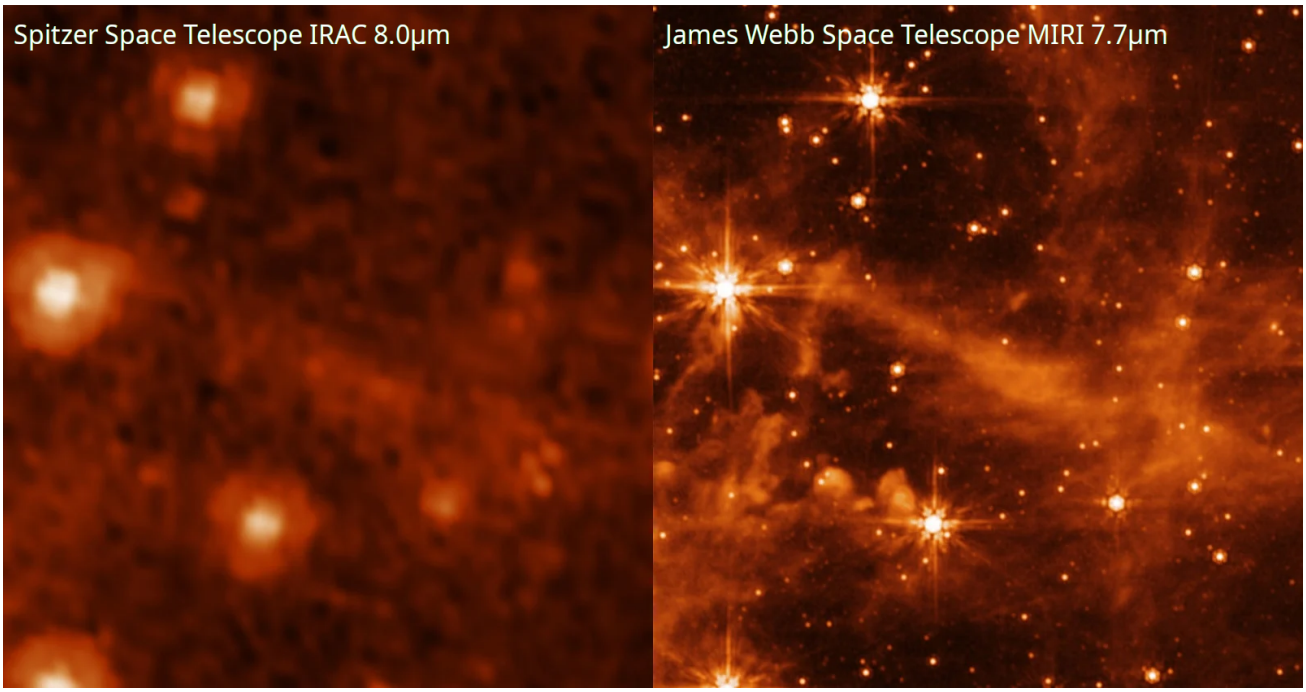

Figure 1: Spitzer Space Telescope IRAC module versus JWST MIRI (pre-commissioning) depth and resolution comparison. Image (and adapted) taken from `https://petapixel.com/2022/05/10/nasa-shows-off-webb-telescope-sharpness-with-comparison-photo`

2 Evolution of a Low - Intermediate Mass Star

Stars with an initial mass in the range of 0.85-8$M_{\odot}$ and solar metallicity (Z$\sim$0.02) will, towards the end of their nuclear-burning life, reside on the asymptotic giant branch (AGB). Exactly how they get there depends on their initial mass but they broadly follow the same evolutionary sequence. What follows is a brief run-through of their journey and some definitions of important terms. See Figure 2 throughout for reference on a sketched H-R diagram.

For the majority of its nuclear-burning life, a star will be sat on the main sequence (MS), a stage of life defined by the fusion of H to He within the core. This stage is very stable but comes to an end once the supply of H is exhausted and the He core contracts to become inert and electron-degenerate. Then begins H-burning a thin shell surrounding the core, which expands and cools the stellar envelope that now becomes convective - causing a subsequent reddening in colour and an increase in luminosity. This process moves the star off the main sequence and onto the red giant branch (RGB). The path from MS to RGB crosses the Hertzsprung Gap, differing stellar properties dictate how they navigate this area but they will all enter the RGB at a similar position. If the convective layer penetrates deeply into the centre of the star, it will dip into the H-burning shell - an event which leads to the "first dredge-up". During this dredge-up, products of the nuclear fusion are brought up to the surface (mostly ^{14}N and ^{13}C).

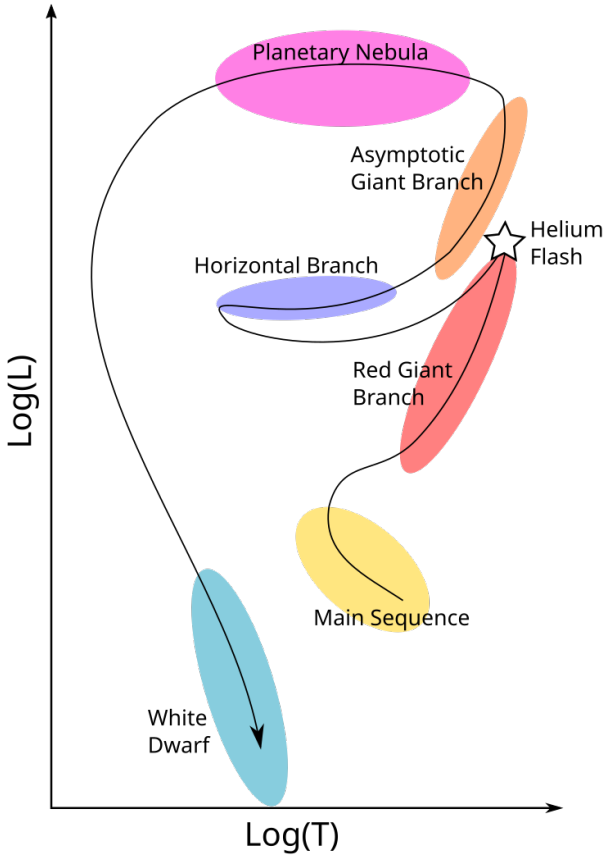

Figure 2: Herztsprung-Russell diagram (sketch), the evolution of a low-intermediate mass, solar metallicity star.

For a time the star is stably H-shell burning and dumping He onto the core and it ascends the RGB until the pressure on the core becomes great enough to overcome its degeneracy and begin the rapid burning of He to C through the 3α process. This event causes a large spike in luminosity and is known as the "helium core flash". This abrupt change moves the star quickly off the RGB and onto either the Red Clump (RC) or the Horizontal Branch (HB) depending on the properties of the star. Younger more massive and metal rich stars form an RC while lower mass old metal poor stars form HBs. After this, it will very stably burn He in the core until its eventual exhaustion, rendering it inert, supported again by electron-degeneracy pressure and consisting of C and O. The stars' main energy source is now supplied by a He-burning shell (in direct contact with the core) and a higher H-burning shell (separated from the He shell by a convective envelope). The star now begins to reascend the giant branch, beginning the Asymptotic Giant Branch phase (O. Jones 2013,Potter et al. 2004,Lattanzio et al. 2004).

2.1 AGB Evolution

While the star is on the AGB it is extremely luminous in the near-infrared and will have a very cool effective temperature (T_{eff}~3500K) (Cami 2002). As it evolves, the star will become brighter and cooler and thus *ascend* the Asymptotic Giant Branch. Throughout this stage, the internal structure of the star will resemble the schematic shown in Figure 3. Although occupying one broadly similar region on an H-R diagram there are two phases to this stage in the stars' evolution; the early-AGB and the thermally pulsing AGB.

2.1.1 Early AGB

The early AGB (E-AGB) phase is defined by the primary burning of the He shell around the core. At this point in time, the core contains nearly $0.5M_{\odot}$ but a radius around $0.02R_{\odot}$ and is entirely degenerate - the upper mass limit of an AGB star ($8M_{\odot}$) is defined physically, above this the core would collapse and initiate C-burning. In intermediate mass AGBs, the convective stellar envelope dips into the top of the H-shell and causes the "second dredge-up" event. Much like the first dredge-up, the event vastly enriches the surface of the star with heavier fused elements. The adjacent He-shell is dumping the ashes of its nuclear burning onto the core and slowly heating the H-shell above it. The star remains in this phase until the H shell is sufficiently hot to start fusing, after which the two shells begin to interact and the nuclear-burning rates will oscillate.

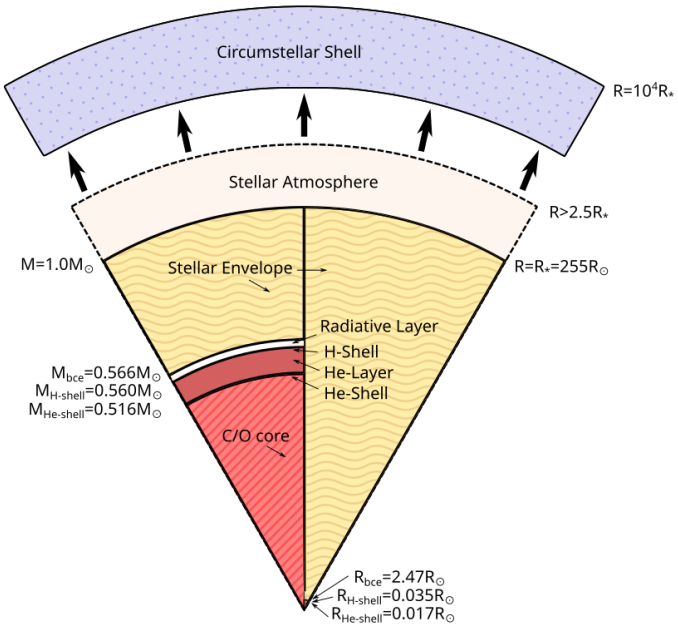

Figure 3: A sketch of the structure of an AGB star and its surrounding dust shell. On the left side of the figure, the internal structure is proportioned by enclosed mass, the right is scaled by enclosed radius. This figure was adapted from (Lattanzio et al. 2004).

2.1.2 Thermally-Pulsing AGB

The shell interactions begin the thermally-pulsing phase of the AGB (TP-AGB). H-burning dumps He onto the shell below, doing so until it is sufficiently hot enough to begin burning. The initiation of this burning creates a lot of energy, developing an inter-shell convective zone and lifting the H-shell to the point at which it cools and ceases burning. The He-burning is short-lived and as the star begins to collapse, this collapse reignites the H-burning and the process repeats

with a period in the order of 10^3-10^4 yrs. During these *thermal pulses*, the convective region in the stellar envelope dips into the shell burning region and initiates the *third dredge-up* event - bringing synthesised carbon from the centre of the star to the surface - playing a vital role in the chemistry of the circumstellar envelope, this is discussed in more detail in Section 2.3. After the first thermal pulse, the once stable star is shocked into instability, causing the star to oscillate[1] with a period of several hundred days. During these oscillations, the effective temperature fluctuates and the peak emission wavelength moves between the infrared and visible, causing variations in the star's luminosity. The onset of the TP-AGB phase initiates huge mass loss from the outer layers of the star in the form of dust driven wind. Eventually, mass loss will disperse the stars' envelope, ending its life on the AGB.

2.2 Long Period Variability

In the 17^{th} century, a dutch astronomer Phocylides Holwarda re-observed a star which had previously disappeared in an event assumed to be similar to a supernova. It was later witnessed to disappear and reappear continually for years, earning the name "Stellar Mira", meaning miraculous (Habing et al. 2004). We know today that this is due to the long period variability during the TP-AGB stage of stellar evolution. Miras are one of a set of classifications that fall under the bracket of stars known as "Long Period Variables" (LPVs). The lightcurves of *"Mira-like"* (M) objects have a large regular periodic amplitude of $\Delta V>2.5$. Lower amplitude and less regular variables are dubbed *"Semiregular Variable"* ("SRV") and have an amplitude $\Delta V<2.5$ with light curves showing both period and irregular behaviour. Finally *"Irregular"* ("L") objects exhibit variability but their light curves are not well constrained.

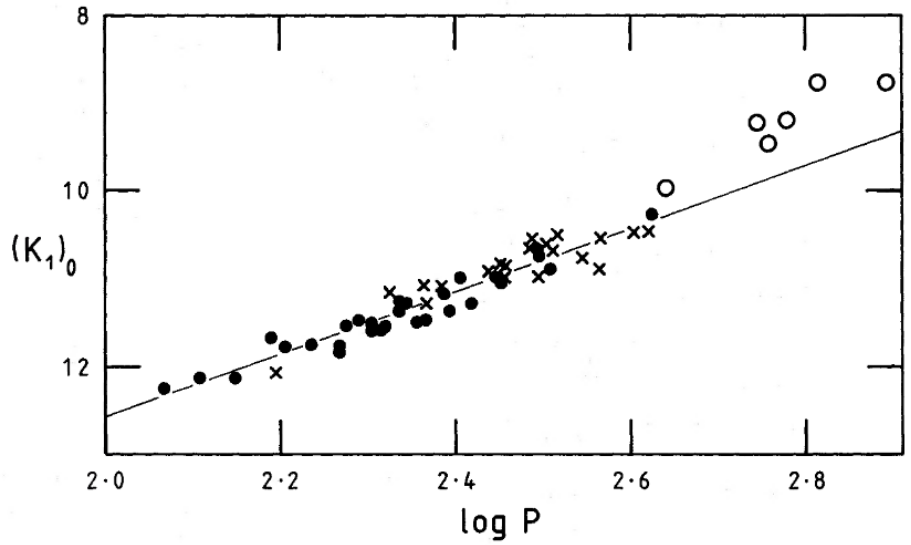

Figure 4: Period-luminosity relation in the K-band: filled circles=O-Miras (P<420d); open circles=O-Miras (P>420d); crosses=C-Miras. The line is the least-squares fit for O and C-Miras with P<420d (Feast et al. 1989)

Light curves of Mira LPVs can be observed with multi-epoch photometry. It was found by (Feast et al. 1989) that the mean K-band luminosity of the curve is tightly constrained with its period. Distributing this data on a log period-magnitude plot, a linear correlation can be fitted with $m_0 = \rho log P + \delta$(Whitelock et al. 2013). This distribution can be seen in Figure 4. The high luminosity end of this figure shows that oxygen rich stars with periods longer than 400 days do

[1]This is continually called pulsation in the literature but is critically different from a thermal pulsation - as such I will call it oscillation from here on.

not quite fall upon this line and is believed to be the effect of the stellar atmospheres (Whitelock et al. 2008). A robust period luminosity relation is a key tool for determining distances to extragalactic objects.

2.3 M and C-type AGB stars

AGB atmospheres have complex elemental abundances and the quantity of carbon determines the stellar classification. Free carbon and oxygen bind to form the very stable CO molecule. The residual element with the higher abundance is counted in the ratio C/O. Stars with a C/O<1 are said to be oxygen rich (O-rich) or in the Harvard system of spectral classification, an M-type star [2]. In the case C/O>1 then it is said to be a C-type star. In the rare case where C/O=1 the star is classified as S-type.

The first of the two main driving forces for the evolution between M- and C-type stars is the aforementioned third dredge-up (TDU). During a TDU event, newly enriched carbon from the core is brought up to the surface, gradually increasing the carbon excess. The second important process is hot bottom burning (HBB), where the base of the convective region converts C to N by means of the CN-cycle, thus limiting the available carbon and increasing the oxygen excess (Garcia-Hernandez et al. 2013). However HBB is unable to occur under low temperatures so is not possible in low mass ($M<2M_{\odot}$) AGBs, as such their surface enrichment is dominated by dredge-ups. Conversely, in high mass ($M>5M_{\odot}$) AGBs the surface chemistry is dominated by HBB as a large portion of the synthesised carbon is converted to nitrogen - limiting the formation of C-type stars. Intermediate mass stars have a contribution from both these effects (Ventura et al. 2021). As a result of the competing processes, it is more likely to find higher mass M-type stars and low mass C-types (Zijlstra et al. 2006)

The photospheric emissions from M- and C-type stars are altered by the differing chemical constituents. This can be detected robustly through spectroscopy - this is however expensive and impractical for wide range surveys. The molecular emissions will present themselves in photometric imaging and the spectral classes are differentiable on a colour-magnitude or a colour-colour diagram. The separation is visualised in Figure 5a, defined by (Cioni et al. 2003), with the inclusion of x-AGB assumed to be a subset of C-type stars.

2.3.1 C/M Ratio

Variations in the number ratio of C- to M-type stars would likely be caused by variations in the metallicity of the natal environment. This is explained by M-type AGBs converting to C-type earlier in lower metallicity because fewer carbon atoms need to be dredged to the surface for the C/O ratio to pass unity. Global metallicity values of nearby objects were compared against global C/M ratios to indeed find a well defined correlation (Cioni et al. 2003), see Figure 5b. This is exploitable on a local level to determine population substructures within galaxies as well as on a global scale. However, it also must be noted that the C/M ratio also depends on the mass dependent star formation rate (Cioni et al. 2006a). It is concluded by (Cioni et al. 2006b) that the SFR must be included in the models to accurately calibrate the metallicity value.

[2]The notation of O-rich vs M-type is broadly interchangeable in the literature. The former is used more frequently in mid-IR studies while the latter is used usually in the context of optical or near-IR studies.

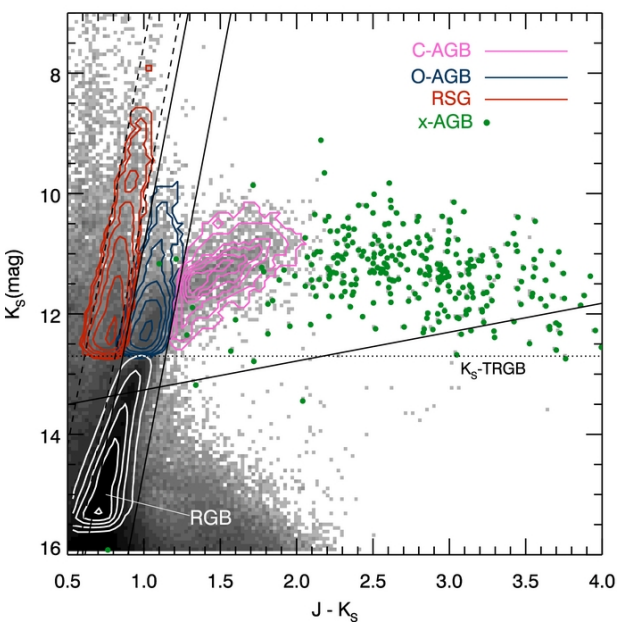

(a) M (O-AGB) and C-type (C-AGB) selection on a colour-magnitude diagram (Martha L. Boyer et al. 2011).

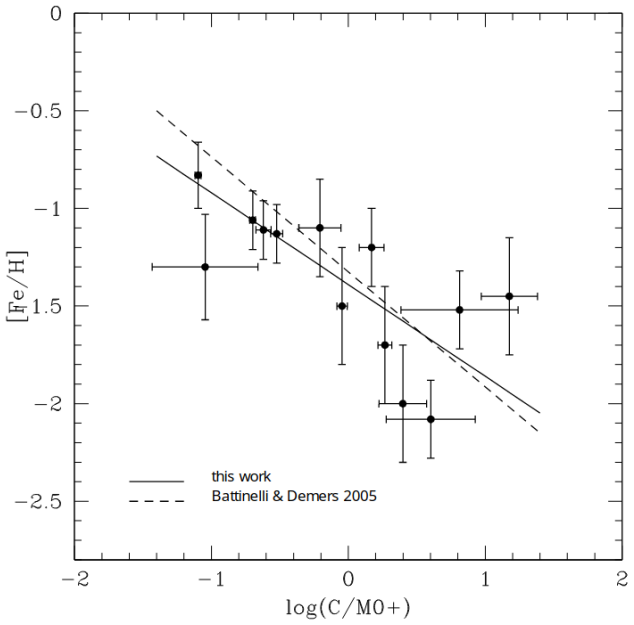

(b) Relation between the metallicity ([Fe/H]) and the C/M ratio. The solid line is a linear fit through the data (Cioni 2009).

Figure 5: Work by (Cioni et al. 2003) to separate M- and C-type stars and then the subsequent use in galactic studies.

2.4 Mass loss and Dust formation

The outer regions of AGB stars are cool (T∼2000-4000K), this allows molecular gas to form in the photosphere. Shock waves from the variability oscillations within the star lift this molecular gas up into the atmosphere, cooling it further (T∼1500K). At a distance of R>2.5R_* (where R_* is the radius of the star, see Figure 3), the temperature is cool enough and density high enough for dust formation to begin through condensation (O. Jones 2013). The radiation pressure from the star has little effect on the molecular gas due to its low opacity but it has a large effect on the condensed dust. The bombarding photons transfer momentum to the dust grains and an outward force is applied. Although only making up a small percentage of the mass (∼1%), the momentum is collisionally transferred from the dust to the surrounding molecular gas and both begin to move outward. The acceleration drops with radius as the force of the radiation pressure decreases, until the material outflow reaches peak velocity, usually taken to be around 10kms^{-1}. Over time, new layers are added and the build up of molecular gas and dust forms the circumstellar shell (Cami 2002).

As the star ascends the AGB, its luminosity (and therefore radiation pressure) increases and temperature decreases, causing an increase in the mass loss rate. At its peak, this will hit rates of $10\text{M}_{\odot}^{-4}\text{yr}^{-1}$, commonly called the *superwind* phase. Stars in this phase are often referred to as *"extreme"* AGBs (x-AGB) and are responsible for a large amount of dust injection into the ISM (Martha L. Boyer et al. 2011).

Dust formation and mass loss are relatively understood in C-type stars as the carbonaceous dust formed are very opaque allowing much lower radiation pressures to drive the wind. However, we have not observed M-type stars with a high enough luminosity to drive the lower opacity silicate dust at the expected rates. It is suspected that embedded iron may be opaque enough to solve this problem but it has not yet been observed (van Loon et al. 2008).

Simulations have been done on the dust formation to determine the key properties that dictate

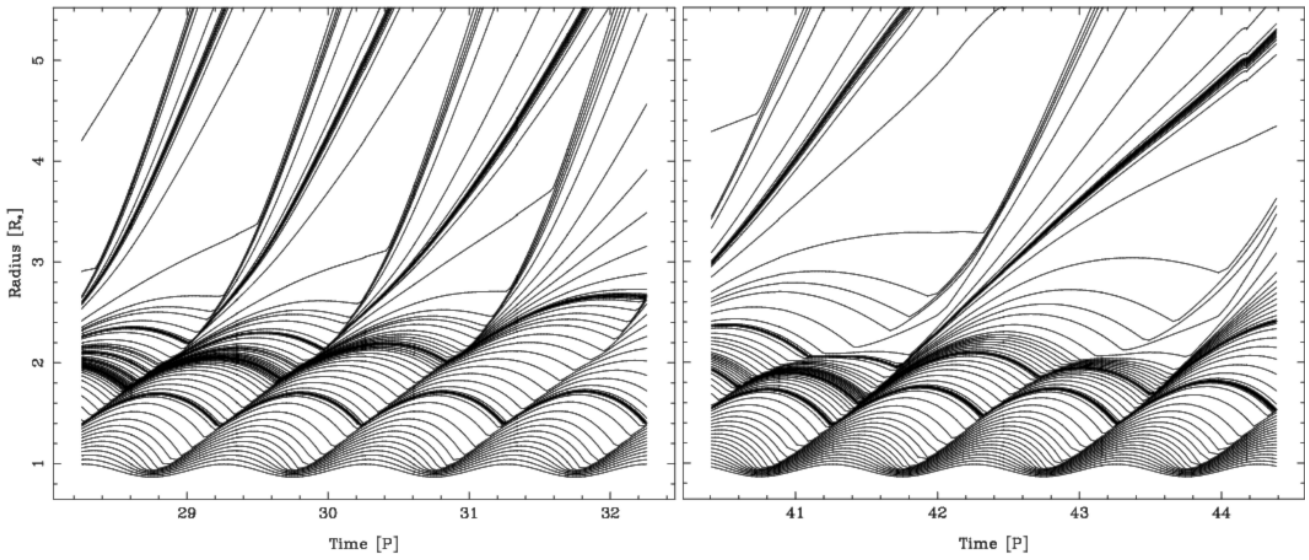

Figure 6: Positions of selected mass shells as a function of time in periodic (left) and multi-periodic (right) cases (Hoefner et al. 1997).

the conditions within the circumstellar shell (Hoefner et al. 1997). It would be expected that after every shock a new layer of mass is lifted out of the star. Although in simple cases this is true, in reality, the new layers form on integer multiples of shocks. This is due to two reasons; dust grain growth is a complex process and the timescales may not align with that of the oscillations, and as the dust shell grows in density and opacity, there also begins self interacting physical systems. A simple case of multi-periodicity would occur in lower density systems where the injection of new matter into the shell doesn't hit a threshold density to begin condensing - as such a second injection is required to trigger it. Figure 6 shows the distance from the centre of the star by a series of test mass shells over time. It is seen that the particles follow the rhythm of the pulsations, gradually moving out until the point that radiation pressure overcomes the reverse gravitational pull. At this point, the shell is lifted irreversibly from the star. The left panel shows a simple periodic case but the right shows how the effects of multi-periodicity effect the mass loss rates. It can be seen in the right panel that the bulk of mass ejection occurs every second oscillation, with the slow growth of matter in the atmosphere in between.

The same simulation (Hoefner et al. 1997) looked at the effect of stellar luminosity and temperature on the mass loss rate. It was observed that by increasing L and decreasing T they could drastically increase the mass loss. The lower temperature allows for more grain formation, and the increased luminosity drives the outflow harder with higher radiation pressure. This result provides a physical mechanism for the observed increase of mass loss as the star ascends the AGB. Additionally, a key result observed in the same simulation was the effect of carbon abundance on mass loss rate. The higher opacity of the carbonaceous grains allows for a greater radiation pressure from the stellar winds to drive the mass loss.

As the circumstellar shell grows, its effect on the light emitted from the photosphere increases. Photons are captured by the gas and dust and then re-radiated in the near-infrared. As the star becomes deeply embedded, this may cause a complete extinction of the optical radiation from the star. The resulting observed spectrum therefore becomes a combination of blackbody (overlaid with molecular) emission from the photosphere, dust and molecular gas absorption features from the circumstellar shell and then re-radiated emission lines. As the opacity of the shell increases, the effects are increased, to the point where emitted radiation from the shell is recaptured before it escapes - a process known as self absorption (Kraemer et al. 2002). Although complicating the photometry of the star, this does allow for detailed studies of its chemical composition.

2.4.1 Circumstellar Shells in M-type AGBs

In M-type AGBs, the abundant oxygen allows for the formation of silicates, molecular OH and water vapour. The heavier Si and Al elements required for the formation of these molecules are not synthesised within the core of the star - instead the unenriched elements are presented with the right conditions to form molecules and dust in the cool dense atmosphere of the star. This makes the abundance of such materials sensitive to the metallicity of the natal environment. As a result, we expect to see a drop in the silicate and alumina dust emissions, as well as the overall number of M-type stars (Sloan et al. 2008).

2.4.2 Circumstellar Shells in C-type AGBs

One of the key molecules detectable within the shell of a C-type star is SiC. It condenses from gas to form conglomerates in cool red dust regions and has a high opacity - as such its formation reduces the incident radiation on the shell, allowing it to cool more. This effect indirectly causes more dust grain formation. Present in most C-type star spectra is an absorption feature caused by acetylene (C_2H_2) - which is a useful method of differentiating them from M-types, in which the feature does not exist (Zijlstra et al. 2006). MgS is also present in cooler C-type AGBs, it expresses itself as a very wide emission in the red side of the spectrum, and it completely obscures the underlying blackbody making it difficult to calculate its excess. MgS is very dependant on metallicity as both elements are not synthesised by the star itself, so its abundance drops rapidly with a decrease in metallicity. Carbon rich dust has a low condensation temperature and high opacity so captured photons cause it to disintegrate, as such it is likely to be destroyed soon after formation and have little effect on the interstellar medium thereafter. However, it is proposed that TiC and SiC may survive long enough to help further grain growth in the future (van Loon et al. 2008).

Unlike their M-type counterparts, C-type AGBs self produce carbon in their cores and dredge up during thermal pulsations. This allows for continual renewal of enriched carbon in the surface chemistry and a resulting increase of carbonaceous material form. This effect makes C-type stars are a lot less sensitive to metallicity, increasing in the C/M ratio as metallicity drops (Sloan et al. 2008).

2.5 Post-AGB Evolution

Shell burning ceases once the stellar wind has ejected the majority of the stellar envelope, reducing it below $\sim 0.01 M_{\odot}$. Subsequent contraction moves the star off the AGB and into the region of post-AGB. During this stage, the wind continues to disperse the circumstellar dust shell and it becomes optically thin enough to observe the core in the centre. The core is extremely hot (T$\sim$30000K) and emits energetic photons in the ultra-violet that ionise the surrounding gas and dust to create a spectacular but short-lived planetary nebula (O. Jones 2013). The hot tiny core burns through all its remaining fuel and then with no remaining method of heating it begins to cool and form a white dwarf (Habing et al. 2004).

3 Galaxy Evolution Through Evolved Stellar Populations

The interstellar medium (ISM) within galaxies is the bank around which its evolution is centred. The ISM contains all the natal material from which new stars form, and receives back once the star dies - enriched by nucleosynthesis to pass onto the next generation. This continual cycle

of baryonic matter drives the evolution of the host galaxy and causes the constant increase of metallicity (M. L. Boyer et al. 2017). To fully understand this process we must understand all its components; formation of new stars from the ISM material, stellar evolution in a range of increasing metal abundances and the material re-injection through evolved stellar mass loss or supernovae. We can gain clues on distant unresolved galaxies in the early universe by studying nearby objects that are compositionally similar. Galaxies with low metallicity and high star formation rates are good analogues to galaxies during the epoch of peak star formation (Hirschauer et al. 2020). By observing objects in the Local Group, we can resolve individual stellar objects, their parent nebula and the remnants left over after the end of their life.

3.1 *Spitzer Space Telescope*

Spitzer has been the most groundbreaking observatory in evolved stellar population studies to date. The 0.85m reflecting telescope was launched in 2003 with imaging capabilities between 3-180μm and a spectroscopic range between 5-40μm and 50-100μm (Werner et al. 2004). This infrared satellite peered into local universe objects to make large strides in our understanding of galaxy evolution, before its decommissioning in 2020. This section reviews some of the most important results from *Spitzer*, which is currently the state-of-the-art observatory in AGB studies

3.1.1 SAGE-LMC

The nearby (∼50kpc) Large Magellanic Cloud (LMC) has a subsolar metallicity (Z∼0.3-0.5Z$_\odot$), approaching the mean ISM metallicity during the peak star forming epoch (Madau et al. 1996). Being a close neighbour to the Milky Way it has been widely studied but (Meixner et al. 2006) pointed *Spitzer* at it to conduct SAGE (Surveying the Agents of a Galaxy's Evolution). SAGE covered the entire LMC with a 7x7 degree field (see Figure 7), to determine evolved star mass loss rates and star formation histories. Studying the evolved sources in the galaxy had previously been biased towards the stars with optically thin shells, owing to an underestimation of mass loss return to the ISM. With the use of the mid-infrared instruments on *Spitzer*, they can observe emissions from the dust shells and identify deeply embedded sources (Sundar Srinivasan et al. 2009).

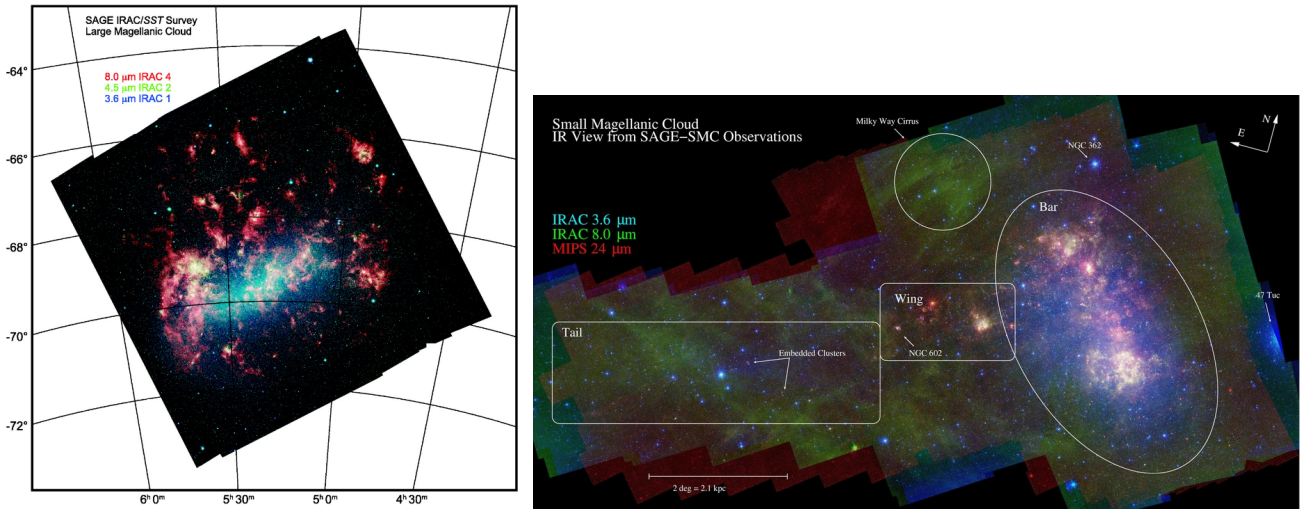

Figure 7: Full coverage of (a) SAGE-LMC (Meixner et al. 2006) and (b) SAGE-SMC (Gordon et al. 2011)

SAGE detected 18000 M-type and 7000 C-type AGBs with a further 1200 completely optically

obscured x-AGB (Blum et al. 2006), giving a stellar C/M ratio from 0.4-0.46 - the upper bound being defined when all x-AGBs sources are being considered C-type. This result agreed and improved the previously wide range 0.2-0.6 (Cioni et al. 2006a). Most of the fainter AGBs had been previously undetected, their cool dusty envelopes and significant mass loss were visible in the 24μm MIPS band. These sources contribute to a large portion of the dust injected into the ISM allowing for a far more detailed picture of the dust life-cycle to be gained.

Empirically proving that AGB mid-infrared colour excess is a good tracer for mass loss rate (Sundar Srinivasan et al. 2009), the mass loss rate increases with luminosity in all IRAC bands. However, a full calibration requires knowledge of the gas-dust ratio (ψ) or only a fraction of the total outflow mass is captured in the calculation. The ratio is expected to increase with a drop in metallicity as the silicate dust abundance decreases, while the carbonaceous dust is less affected. Assuming a Galactic gas-dust ratio for C-type stars ψ=500 and taking the M-type ratio ψ=200, they calculate the mass loss rate to be 4.8×10^{-4}M$_\odot$yr^{-1} and 7×10^{-4} M$_\odot$yr^{-1}respectively. The exact spectral classification of the x-AGB population is difficult to determine as the emission is significantly obfuscated by the enshrouding dust, the gas-dust ratio is then drawn from a range and the total mass loss rate is between 4.7-11.8$\times10^{-3}$ M$_\odot$yr^{-1}. The three classifications combined bring the total mass loss rate to 5.9-13x10^{-3}M$_\odot$yr^{-1} (Sundar Srinivasan et al. 2009). Constraining the value more would require further detailed studies on classifying the exact spectral class of the x-AGB population.

In the third paper of the series (Whitney et al. 2008) the SAGE team use young stellar objects (YSOs) to calculate the current star formation rate (SFR) in the galaxy. By calculating the YSOs total mass and luminosity and comparing it to the initial mass function, they arrive at a current SFR of $\sim$0.06M$_\odot$yr^{-1}. This value is an order of magnitude higher than the mass loss return rate described above. This imbalance would lead to the complete consumption of the ISM (if it were an isolated system) in timescales shorter than the age of the LMC. Instead, AGB mass loss is supplemented by the higher mass RSGs and supernovae. An alternative explanation (or additional component) may come from material in-fall from tidal stripping of the Small Magellanic Cloud through the adjoining bridge.

3.1.2 SAGE-SMC

After SAGE-LMC came the sister study on the Small Magellanic Cloud (SAGE-SMC) (Gordon et al. 2011). The SMC is similarly nearby ($\sim$60kpc) but has a lower metallicity than the LMC (Z$\sim$0.2-0.3Z$_\odot$), aligning it with the conditions present during the peak star forming epoch. The two surveys were thus used to explore the influence of metallicity on a galactic scale. The primary goal of this survey was to calculate the total dust in the ISM, studying its full life cycle.

While separating C-type and M-type sources, an anomalous region on the M-type zone of the J-8 vs M$_8$ CMD was identified, which was dubbed aO-rich (Martha L. Boyer et al. 2011). These sources are characterised as belonging clearly to the M-type class but being redder than the proposed cut-off: $[8] = 27.95 - (11.76 \times J - [8])$. This population is proposed to be M-type stars that are forming large amounts of dust.

Using the infrared colour excess as before but this time mass loss rates are calibrated against SMC stars in the dataset, with known radiative transfer models. S. Srinivasan et al. 2016 find the global value to be within the range 1.6-3.98x10^{-6}M$_\odot$yr-1, some 7 times lower than the LMC. They identify 4.5% of the population to be x-AGB but calculate the individual mass-loss rate as 5 times higher than "standard" C-types in the galaxy and some 300 times higher than M-types. Consequently they are the primary dust producer in the SMC. It is proposed that the low metallicity environment of the SMC prevents the M-type AGBs to produce sufficient dust to drive the outflow wind(M. L. Boyer et al. 2011).

3.1.3 DUSTINGS

SAGE allowed for the comparison between Z=0.2-0.5$Z_{\odot}$environments, giving us a confined example of how the population properties of evolved stars may differ with metallicity but a more general picture would require far more galaxies to study. DUSTINGS (DUST in Nearby Galaxies with *Spitzer*) was a survey covering 50 dwarf galaxies in the Local Group, out to a distance of 1.5 Mpc. Specifically, it aimed to identify the evolved and massive populations. The photometry of the survey reached down to the tip of the RGB at 75% completeness, allowing robust wide scale statistical analysis of the populations. The survey spans a wide range of metallicity environments (-2.7 <[Fe/H] <-1.0) (Martha L. Boyer et al. 2015a).

Using some of these extremely low metallicity galaxies, DUSTINGS aimed to show, by analogy, the dust production in the high redshift universe. They identify 12 x-AGB stars in galaxies with [Fe/H]<-2.0, and then show that the dust production rate of these C-type x-AGBs is independent of metallicity. This result highlighted the importance of AGB stars in the ISM enrichment of early universe galaxies (Martha L. Boyer et al. 2015b). However, in many cases, the C-type stars are lower mass and spend a long time on the main sequence before producing dust. The higher mass (M>4$M_{\odot}$) AGBs that undergo hot bottom burning are likely to be M-type, although their dust production rate is limited by lower metallicity (Sloan et al. 2008), their shorter lifetimes would allow for faster injection of dust into the ISM. DUSTINGS found 26 dust producing M-type stars within the sample that could start producing dust as early as 30 Myr, the brightest of which has an inferred mass (12$M_{\odot}$) exceeding the theoretical mass limit of an AGB (M. L. Boyer et al. 2017).

4 Progress to Date

JWST begins observing and releasing data in the summer of 2022, early images indicate an unprecedented level of sensitivity (see Figure 1). It is expected to mark a turning point in galaxy evolution as it observes the birth of galaxies in the early universe and Local Group resolved studies in remarkable detail. Whereas *Spitzer* might resolve the tip of the RGB at 1 Mpc (Martha L. Boyer et al. 2015a), it is expected that *JWST* will resolve the red clump or main sequence turn off. This depth will allow for full star formation history studies.

The increase in sensitivity is expected to be groundbreaking, the primary mirror is 6.5m compared to *Spitzers'* 0.85m. We have already seen a preview of the quality (Figure 1) but Figure 8 shows more technical details. Across the full range of *JWSTs'* observing spectrum, it drastically improves the limiting flux with respect to every major observatory before it. The hope is that we will be able to capture stellar populations much farther down the H-R diagram and the most deeply embedded dusty objects.

My PhD work will involve analysis of early data from *JWST*, specifically guaranteed time observations of two nearby galaxies, NGC 6822 and 1 Zw 18.

4.1 PSF Photometry pipeline

To prepare for scientific analysis of *JWST* data, it is necessary to develop and validate software and tools. As part of the images received from JWST, an aperture photometry catalogue of the sources in the image will be included. Aperture photometry although being a fast method of reducing an image will be insufficient for the densely crowded fields we expect to see in resolved local group objects. Point spread function (PSF) photometry is the fitting of a telescope's unique normalised PSF to the sources in the image and allows very accurate photometry when crowding

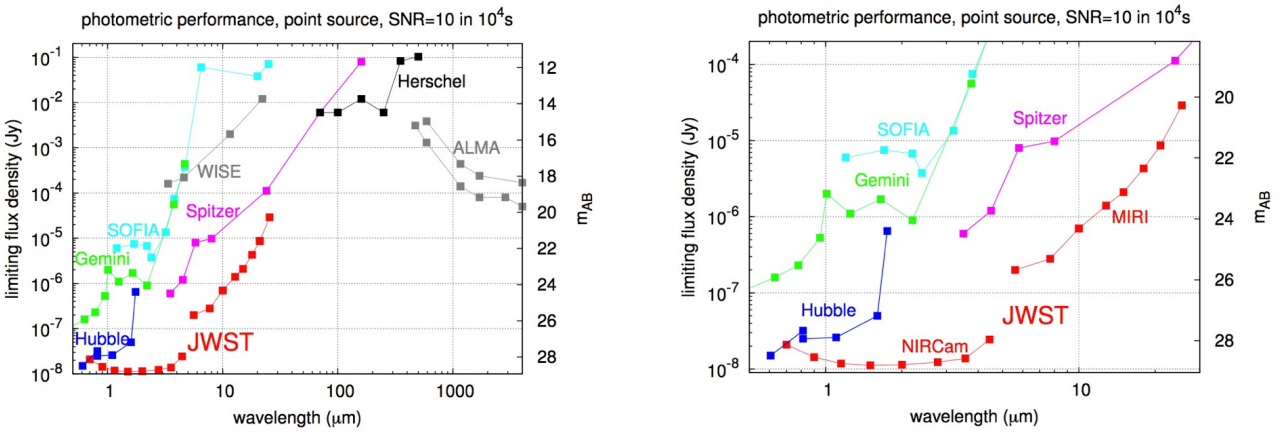

Figure 8: caption `https://www.stsci.edu/jwst/about-jwst/history/historical-sensitivity-estimates`

causes several stars to overlap along the line of sight. Many well tested PSF photometry tools exist. DAOPHOT (Stetson 1987) is a telescope independent tool that has been in use for decades, however, it is archaic in its usability and doesn't allow for the inclusion of the incredibly well-modelled PSF of JWST (Figure 9a). DOLPHOT (Dolphin 2016) is a widely used and robust tool but it is designed for HST and the diffuse emissions that will be present in the mid-infrared MIRI images from JWST will play havoc with its detection and fitting. As a result of this, I have set out to write a python based PSF photometry tool specifically designed to integrate with the JWST images. It is written using Astropy (Astropy Collaboration et al. 2013) and Photutils (Bradley et al. 2020) allowing it to be easily customisable for anyone with the source code.

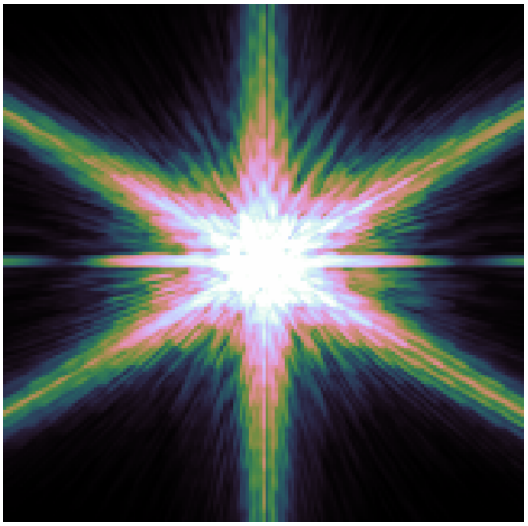

(a) JWST F444W PSF.

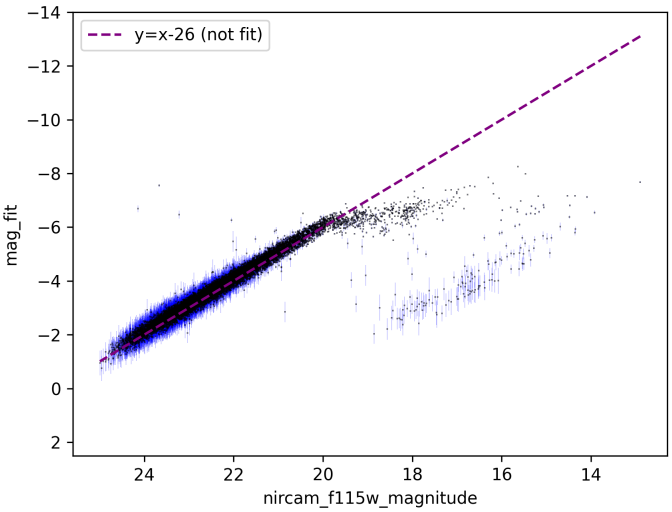

(b) Starbug input-output comparison on simulated NIRCAM data. Along the horizontal axis is the catalogue of input magnitudes into the simulated data and the vertical axis shows the calculated magnitudes from StarBug.

Figure 9: Current progress of Starbug PSF fitting tool.

The tool (currently called Starbug) contains a full suite of PSF photometry tools: source detection, PSF fitting, catalogue cleaning and matching, and full artificial star testing. To combat the diffuse emissions in the infrared, Starbug runs an ensemble of background subtraction tech-

niques and builds several source lists from the residual images, combining them to form one large catalogue. Forced position PSF fitting is then run using a routine emulating DAOPHOT to create the photometry catalogue.

Running Starbug on simulated JWST Nircam images, it can recover the input source list with a high degree of accuracy (Figure 9b). There are however still some problems, at the high luminosity end where the pipeline underestimates the flux of the brightest sources - this is believed to be some saturation effects in the data.

4.2 Preparatory Work for Euclid

Planned for roughly a year after the launch of *JWST* is *Euclid* (Laureijs et al. 2011), the optical to near-infrared surveying telescope. With results gained from the *JWST* programs, we will be able to test new theories on a far wider field. I have joined the "Extragalactic Stellar Populations Working Package" and have begun exploratory work in simulated isochrones. Primarily this has involved defining expected observable stellar populations within different environments, for example; what is the most distant globular cluster that Euclid has the sensitivity to observe the tip of the RGB? Figure 10 shows a brief example of measuring the separation between 10 Gyr populations with [M/H]=(-2,-1) at the tip of the RGB and main sequence turn off, in combinations of Euclid photometric bands. These range of exercises will be used in observation proposals once the telescope has been launched.

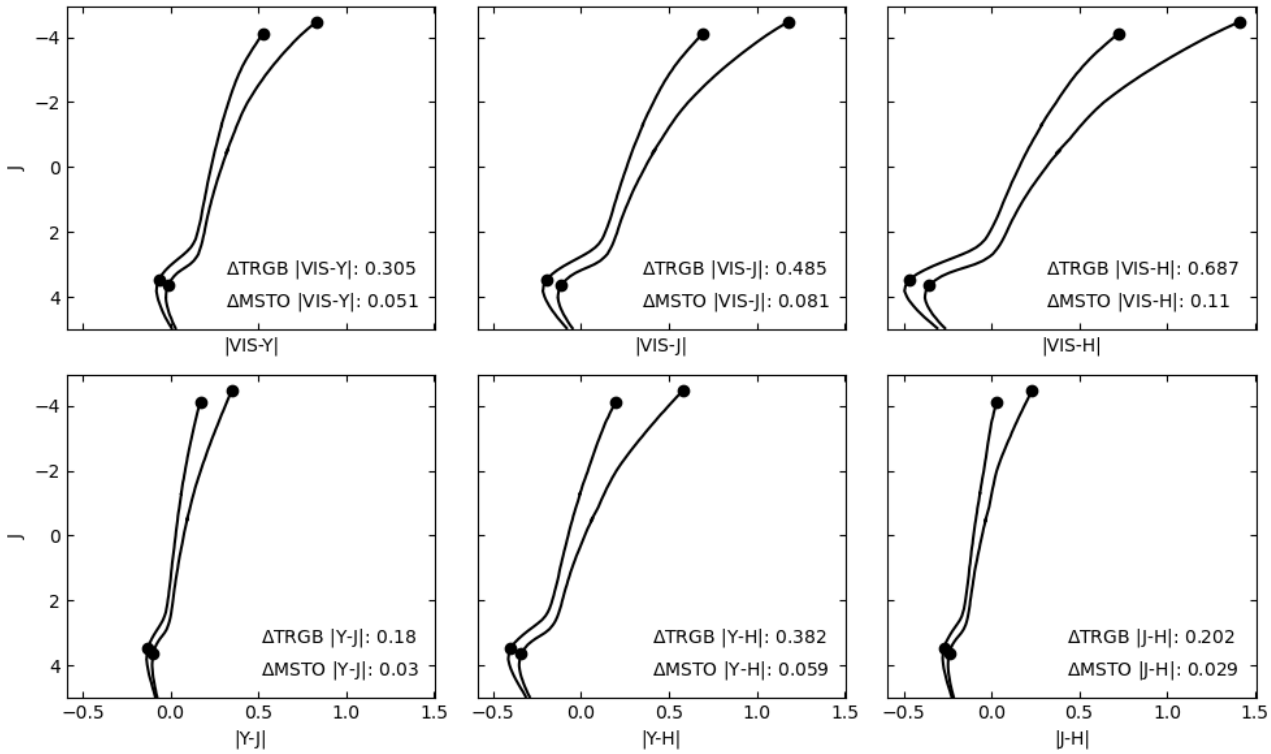

Figure 10: Main sequence turn off and tip of the RGB separations in colour-space between Euclid photometric band pairs.

5 Proposal

Once JWST commissioning is complete, we are involved in four GTO programs. These include resolved studies of Local Group objects: NGC 6822, 1Zw18, NGC 346 and N79. The evolved stellar population within NGC 6822 will be identified and used to compare the chemical enrichment and star formation history to the SMC.

5.1 NGC 6822

NGC 6822 is an isolated barred dwarf irregular galaxy in the Local Group ($\sim$500kpc). The galaxy is relatively low metallicity Fe/H$\sim$-1.2 (Z=0.3Z$_\odot$), similar to the Small Magellanic Cloud. The metallicity is like that of galaxies during the peak star forming epoch (z$\sim$2) and is currently undergoing constant active star formation (Hirschauer et al. 2020). The galaxy has a large healthy population of evolved stars (Whitelock et al. 2013) and several recently identified star forming zones in the central region (O. C. Jones et al. 2019). This paired with the convenient fact that it is isolated makes it an excellent analogue for early universe star forming galaxies.

5.2 1 Zw 18

1 Zw 18 is the most metal poor blue compact dwarf galaxy known (Z$\sim$1/50Z$_\odot$). At a distance of 12 Mpc, it has been difficult to conduct significant resolved surveys on. It is known to be undergoing a star forming episode, with a significant young (age<30 Myr) but also evolved populations with maximum ages of 500 Myr. It was observed with HST, or rather, not observed, that the RGB population is not present despite Hubble sensitivity being fine enough to detect such a population. The conclusion drawn from this is that 1 Zw 18 is a very young (age<500 Myr) galaxy (Izotov et al. 2004). 1 Zw 18 is therefore, a perfect analogue to some of the earliest galaxies in the universe.

5.3 Initial Work

When the images are in-hand, I will reduce NGC6822 images and use NIRCAM and MIRI filters to identify optimal combinations for stellar population separation. This will be used to produce a combined catalogue and CMD paper that will be subsequently used for the rest of the program. The aim would be to define the new standard filter set to separate M- and C-type AGBs, RSGs and (if applicable) RC populations in low (SMC-like) environments. PARSEC (Bressan et al. 2012) stellar evolutionary models can be gained ahead of time to estimate the ideal set and quickly verified after the images are reduced...

5.4 Following Work

Once the catalogue has been compiled for NGC6822, the project could go down a number of lines. Identifying the M- and C-type AGBs and comparing their similarities and differences to the SMC to gain an insight into the chemistry of the galaxy. Measuring the total mass loss within the galaxy to help understand how dust was recycled during the peak star forming epoch. Using the AGB population as a tracer for intermediate age star formation rates and RSGs for the recent SFR. If the data is sensitive enough to capture the red clump or main sequence turn-off, then we will be able to infer the full star formation history of the galaxy and how it differs within different regions of the galaxy.

While I will focus primarily on the evolved populations in these local group objects, members of the program teams aim to study the YSOs in the same regions. Being part of this team will offer a wide view of the full history of the galaxy.

6 Summary

Data from *JWST* during its first observation cycle of four Local Group galactic objects will be taken and the evolved stellar populations identified. These will be used to infer galactic properties and compared against existing results to aid in the understanding of dust enrichment at higher redshifts.

Bibliography

Astropy Collaboration et al. (Oct. 2013). "Astropy: A community Python package for astronomy". In: A&A 558, A33, A33. DOI: 10.1051/0004-6361/201322068. arXiv: 1307.6212 [astro-ph.IM].

Blum, R. D. et al. (Nov. 2006). "Spitzer SAGE Survey of the Large Magellanic Cloud. II. Evolved Stars and Infrared Color-Magnitude Diagrams". In: AJ 132.5, pp. 2034–2045. DOI: 10.1086/508227. arXiv: astro-ph/0608189 [astro-ph].

Boyer, M. L. et al. (Sept. 2011). "A SAGE Overview of AGB Stars in the Small Magellanic Cloud". In: *Why Galaxies Care about AGB Stars II: Shining Examples and Common Inhabitants*. Ed. by F. Kerschbaum et al. Vol. 445. Astronomical Society of the Pacific Conference Series, p. 473.

Boyer, M. L. et al. (Dec. 2017). "An Infrared Census of DUST in Nearby Galaxies with Spitzer (DUSTiNGS). IV. Discovery of High-redshift AGB Analogs". In: ApJ 851.2, 152, p. 152. DOI: 10.3847/1538-4357/aa9892. arXiv: 1711.02129 [astro-ph.SR].

Boyer, Martha L. et al. (Oct. 2011). "Surveying the Agents of Galaxy Evolution in the Tidally Stripped, Low Metallicity Small Magellanic Cloud (SAGE-SMC). II. Cool Evolved Stars". In: AJ 142.4, 103, p. 103. DOI: 10.1088/0004-6256/142/4/103. arXiv: 1106.5026 [astro-ph.SR].

Boyer, Martha L. et al. (Jan. 2015a). "An Infrared Census of Dust in nearby Galaxies with Spitzer (DUSTiNGS). I. Overview". In: ApJS 216.1, 10, p. 10. DOI: 10.1088/0067-0049/216/1/10. arXiv: 1411.4053 [astro-ph.GA].

Boyer, Martha L. et al. (Feb. 2015b). "An Infrared Census of DUST in Nearby Galaxies with Spitzer (DUSTiNGS). II. Discovery of Metal-poor Dusty AGB Stars". In: ApJ 800.1, 51, p. 51. DOI: 10.1088/0004-637X/800/1/51. arXiv: 1412.0695 [astro-ph.GA].

Bradley, Larry et al. (Sept. 2020). *astropy/photutils: 1.0.0*. Zenodo. Version 1.0.0. DOI: 10.5281/zenodo.4044744.

Bressan, Alessandro et al. (Nov. 2012). "PARSEC: stellar tracks and isochrones with the PAdova and TRieste Stellar Evolution Code". In: MNRAS 427.1, pp. 127–145. DOI: 10.1111/j.1365-2966.2012.21948.x. arXiv: 1208.4498 [astro-ph.SR].

Cami, J (2002). "Molecular gas and dust around evolved stars". PhD thesis. University of Amsterdam.

Cioni, M. -R. L. (Nov. 2009). "The metallicity gradient as a tracer of history and structure: the Magellanic Clouds and M33 galaxies". In: A&A 506.3, pp. 1137–1146. DOI: 10.1051/0004-6361/200912138. arXiv: 0904.3136 [astro-ph.CO].

Cioni, M. -R. L. et al. (Apr. 2003). "AGB stars in the Magellanic Clouds. I. The C/M ratio". In: A&A 402, pp. 133–140. DOI: 10.1051/0004-6361:20030226. arXiv: astro-ph/0302051 [astro-ph].

Cioni, M. -R. L. et al. (Mar. 2006a). "AGB stars in the Magellanic Clouds. II. The rate of star formation across the LMC". In: A&A 448.1, pp. 77–91. DOI: 10.1051/0004-6361:20053933. arXiv: astro-ph/0509881 [astro-ph].

– (June 2006b). "AGB stars in the Magellanic Clouds. III. The rate of star formation across the Small Magellanic Cloud". In: A&A 452.1, pp. 195–201. DOI: 10.1051/0004-6361:20054699. arXiv: astro-ph/0602483 [astro-ph].

Dolphin, Andrew (Aug. 2016). *DOLPHOT: Stellar photometry*. Astrophysics Source Code Library, record ascl:1608.013. ascl: 1608.013.

Feast, M. W. et al. (Nov. 1989). "A period-luminosity-colour relation for Mira variables." In: MNRAS 241, pp. 375–392. DOI: 10.1093/mnras/241.3.375.

Garcia-Hernandez, D. A. et al. (July 2013). "Hot bottom burning and s-process nucleosynthesis in massive AGB stars at the beginning of the thermally-pulsing phase". In: A&A 555, L3, p. L3. DOI: 10.1051/0004-6361/201321818. arXiv: 1306.2134 [astro-ph.SR].

Gordon, K. D. et al. (Oct. 2011). "Surveying the Agents of Galaxy Evolution in the Tidally Stripped, Low Metallicity Small Magellanic Cloud (SAGE-SMC). I. Overview". In: AJ 142.4, 102, p. 102. DOI: 10.1088/0004-6256/142/4/102. arXiv: 1107.4313 [astro-ph.CO].

Habing, Harm J. et al. (2004). "AGB Stars: History, Structure, and Characteristics". In: *Asymptotic Giant Branch Stars*. Springer, pp. 1–21. DOI: 10.1007/978-1-4757-3876-6_1.

Hirschauer, Alec S. et al. (Apr. 2020). "Dusty Stellar Birth and Death in the Metal-poor Galaxy NGC 6822". In: ApJ 892.2, 91, p. 91. DOI: 10.3847/1538-4357/ab7b60. arXiv: 2002.12437 [astro-ph.GA].

Hoefner, S. et al. (Mar. 1997). "Dust formation in winds of long-period variables. IV. Atmospheric dynamics and mass loss." In: A&A 319, pp. 648–654.

Izotov, Yuri I. et al. (Dec. 2004). "Deep Hubble Space Telescope ACS Observations of I Zw 18: a Young Galaxy in Formation". In: ApJ 616.2, pp. 768–782. DOI: 10.1086/424990. arXiv: astro-ph/0408391 [astro-ph].

Jones, O (2013). "Dust production by evolved stars in the Local Group". PhD thesis. University of Manchester.

Jones, Olivia C. et al. (Nov. 2019). "The young stellar population of the metal-poor galaxy NGC 6822". In: MNRAS 490.1, pp. 832–847. DOI: 10.1093/mnras/stz2560. arXiv: 1909.03884 [astro-ph.GA].

Kraemer, Kathleen E. et al. (June 2002). "Classification of 2.4-45.2 Micron Spectra from the Infrared Space Observatory Short Wavelength Spectrometer". In: ApJS 140.2, pp. 389–406. DOI: 10.1086/339708. arXiv: astro-ph/0201507 [astro-ph].

Lattanzio, John C. et al. (2004). "Evolution, Nucleosynthesis, and Pulsation of AGB Stars". In: *Asymptotic Giant Branch Stars*. Springer, pp. 23–104. DOI: 10.1007/978-1-4757-3876-6_2.

Laureijs, R. et al. (Oct. 2011). "Euclid Definition Study Report". In: *arXiv e-prints*, arXiv:1110.3193, arXiv:1110.3193. arXiv: 1110.3193 [astro-ph.CO].

Madau, Piero et al. (Dec. 1996). "High-redshift galaxies in the Hubble Deep Field: colour selection and star formation history to z~4". In: MNRAS 283.4, pp. 1388–1404. DOI: 10.1093/mnras/283.4.1388. arXiv: astro-ph/9607172 [astro-ph].

Meixner, Margaret et al. (Dec. 2006). "Spitzer Survey of the Large Magellanic Cloud: Surveying the Agents of a Galaxy's Evolution (SAGE). I. Overview and Initial Results". In: AJ 132.6, pp. 2268–2288. DOI: 10.1086/508185. arXiv: astro-ph/0606356 [astro-ph].

Potter, C. et al. (June 2004). "Book review: Asymptotic Giant Branch Stars (Habing & Olofsson)". In: *Journal of the British Astronomical Association* 114, p. 168.

Sloan, G. C. et al. (Oct. 2008). "The Magellanic Zoo: Mid-Infrared Spitzer Spectroscopy of Evolved Stars and Circumstellar Dust in the Magellanic Clouds". In: ApJ 686.2, pp. 1056–1081. DOI: 10.1086/591437. arXiv: 0807.2998 [astro-ph].

Srinivasan, S. et al. (Apr. 2016). "The evolved-star dust budget of the Small Magellanic Cloud: the critical role of a few key players". In: MNRAS 457.3, pp. 2814–2838. DOI: 10.1093/mnras/stw155. arXiv: 1601.04710 [astro-ph.SR].

Srinivasan, Sundar et al. (June 2009). "The Mass Loss Return from Evolved Stars to the Large Magellanic Cloud: Empirical Relations for Excess Emission at 8 and 24 μm". In: AJ 137.6, pp. 4810–4823. DOI: 10.1088/0004-6256/137/6/4810. arXiv: 0903.1661 [astro-ph.CO].

Stetson, Peter B. (Mar. 1987). "DAOPHOT: A Computer Program for Crowded-Field Stellar Photometry". In: PASP 99, p. 191. DOI: 10.1086/131977.

van Loon, J. Th. et al. (Sept. 2008). "Molecules and dust production in the Magellanic Clouds". In: A&A 487.3, pp. 1055–1073. DOI: 10.1051/0004-6361:200810036. arXiv: 0806.3557 [astro-ph].

Ventura, P. et al. (Nov. 2021). "Gas and dust from extremely metal-poor AGB stars". In: A&A 655, A6, A6. DOI: 10.1051/0004-6361/202141017. arXiv: 2108.04471 [astro-ph.SR].

Werner, M. W. et al. (Sept. 2004). "The Spitzer Space Telescope Mission". In: *The Astrophysical Journal Supplement Series* 154.1, pp. 1–9. DOI: 10.1086/422992. URL: https://doi.org/10.1086/422992.

Whitelock, Patricia A. et al. (May 2008). "AGB variables and the Mira period-luminosity relation". In: MNRAS 386.1, pp. 313–323. DOI: 10.1111/j.1365-2966.2008.13032.x. arXiv: 0801.4465 [astro-ph].

Whitelock, Patricia A. et al. (Jan. 2013). "The Local Group galaxy NGC 6822 and its asymptotic giant branch stars". In: MNRAS 428.3, pp. 2216–2231. DOI: 10.1093/mnras/sts188. arXiv: 1210.3695 [astro-ph.GA].

Whitney, B. A. et al. (July 2008). "Spitzer Sage Survey of the Large Magellanic Cloud. III. Star Formation and ~1000 New Candidate Young Stellar Objects". In: AJ 136.1, pp. 18–43. DOI: 10.1088/0004-6256/136/1/18.

Zijlstra, Albert A. et al. (Aug. 2006). "A Spitzer mid-infrared spectral survey of mass-losing carbon stars in the Large Magellanic Cloud". In: MNRAS 370.4, pp. 1961–1978. DOI: 10.1111/j.1365-2966.2006.10623.x. arXiv: astro-ph/0602531 [astro-ph].